International Journal of High-Rise Buildings
December 2019, Vol 8, No 4, 313-324
https://doi.org/10.21022/IJHRB.2019.8.4.313

International Journal of
High-Rise Buildings
www.ctbuh-korea.org/ijhrb/index.php

Investigation of Typhoon Wind Speed Records on Top of a Group of Buildings

Min Liu[1], Yi Hui[1†], Zhengnong Li[2], and Ding Yuan[1]

[1]School of Civil Engineering, Chongqing University, Chongqing, China
[2]College of Civil Engineering, Hunan University, Hunan, China

Abstract

This paper presents the analysis of wind speeds data measured on top of three neighboring high-rise buildings close to a beach in Xiamen city, China, during Typhoon "Usagi" 2013. Wind tunnel simulation was carried out to validate the field measurement results. Turbulence intensity, turbulence integral scale, power spectrum and cross correlation of recorded wind speed were studied in details. The low frequency trend component of the typhoon speed was also discussed. The field measurement results show turbulence intensity has strong dependence to the wind speed, upwind terrain and even the relative location to the Typhoon center. The low frequency fluctuation could severely affect the characteristics of wind. Cross correlation of the measured wind speeds on different buildings also showed some dependence on the upwind terrain roughness. After typhoon made landfall, the spatial correlation of wind speeds became weak with the coherence attenuating quickly in frequency domain.

Keywords: High-rise building, Field measurement, Typhoon, Wind characteristics, Cross correlation

1. Introduction

Several typhoons generated from the Pacific Ocean can affect China every year. The coastal areas are usually well developed with many high-rise buildings constructed. The knowledge on the wind characteristics of typhoon and its effects on high-rise buildings become more and more important for engineers and researchers (e.g., Li et al., 2016; Li and Li, 2019). Such knowledge provides the basis to reproduce or simulate the strong wind events and their effects on structures by wind tunnel or computer program in further research.

To better understand the wind characteristics of Typhoon, a number of measurements have been conducted near top of structures or over open flat smooth land under typhoon or hurricane conditions (e.g., Fu et al., 2008; Cao et al., 2009; Hui et al., 2009a, 2009b; Masters et al., 2010; Wang et al., 2011). Schroeder et al. (2003; 2009) studied the characteristics such as the wind speeds, roughness length, turbulence intensities, gust factors, and integral length scales of typhoon flow field near the ground, in which the non-stationary wind characteristics were also checked. Vickery and Skerjl (2005) analyzed the land and ocean based weather systems and hurricane gust factors. They suggested that in most cases hurricane gust factors can be described using models developed for standard neutral boundary layer flow conditions. In order to study the wind effects on high-rise buildings, Li et. al. (2005) presented the field measurement results of wind characteristics on top of two super-tall buildings in Hong Kong and Shenzhen. Wind direction dependent analysis was conducted on the wind characteristics of typhoon (Tamura et al., 1993; Xu and Zhan, 2001). Besides the studies based on conventional anemometers, scholars also tried to analyze typhoon based on remote sensing system such as Doppler Sodar (Tse et al., 2013, 2014; Li et al., 2014). Wang et al. (2013) adopted 3D ultrasonic anemometers to collect wind data from three strong wind events (including two typhoons) to study the mean wind speed and direction, turbulence intensity, turbulence integral scale, and power spectral density of wind.

Although there have been extensive researches on characteristics of Typhoon and the effects of Typhoon on tall buildings, there is still lack of information about the structures and characteristics of Typhoons over land for the wind-resistant design of high-rise structures (Holmes, 2010; Kijewski-Correa et al., 2013; Yoshida and Tamura, 2015; Li and Li, 2019). Besides most of measurements are on one high-rise building. Studies attempt to investigate the characteristics of the spatial property of wind by records on some neighboring high-rise buildings may give some more useful information. This study provides a sample and investigates the characteristics of wind speeds measured on the top of three closely spaced buildings in Xiamen city, China during the whole event with the passage of Typhoon "Usagi" close to Xiamen city. The characteristics

†Corresponding author: Yi Hui
Tel: 8602365120720 ; Fax: 8602365120720
E-mail: alihui@cqu.edu.cn

of wind speed including turbulence intensity, turbulence integral scale and power spectrum are investigated. The non-stationarity property and spatial correlation of wind are studied in this study.

This paper is arranged as follows. Setup and field measurement is presented in section 2. The validation by wind tunnel test for excluding possible data pollution and selecting rational data is presented in section 3. The basic characteristics of wind speed including turbulence intensity, turbulence integral scale and power spectrum are given in section 4. Specially, the cross correlation of wind speed by a developed method of evaluating coherence function is presented in section 5. Finally, some conclusions are given in section 6.

2. Setup of field measurement

The measuring site is located less than 600 meters from the sea (Figure. 1). There are only roads and some low-rise buildings between beach and the three buildings in the east, so there is almost no obstacle in front of the buildings when the wind approaches from the east. The other three sides of the buildings are surrounded by Xiamen City. Across the bay in the northeast side of measuring site is also part of the city. The three buildings are named as Buildings A, B, and C as shown in Figure. 1(b) and Figure. 2, which are 97.5 m, 105.3 m, and 143.4 m high. They all have the dimensions of 60 m × 30 m in plan. The orientation of Building-C is perpendicular to the other two buildings (Figure. 2).

Propeller type anemometers (Type 05103V) made by R.M. Yong company were installed on top of each building at the positions indicated by pentagrams in Figure. 2. They were mounted 4.2 m above the top of the fence, and totally 10.6 m above the roof (Height of Fence is 3 m, Height of parapet is 3.4m), as shown in Figure. 2.

The anemometer is designed to withstand maximum 100 m/s gust. Its four-blade polypropylene helicoids propellers have distance constant "λ" of 2.7 m for wind speed. Distance constant λ is an dynamic response indicator



(a) Top view of measuring site (b) Photo of buildings

Figure 1. Measurement site and buildings.

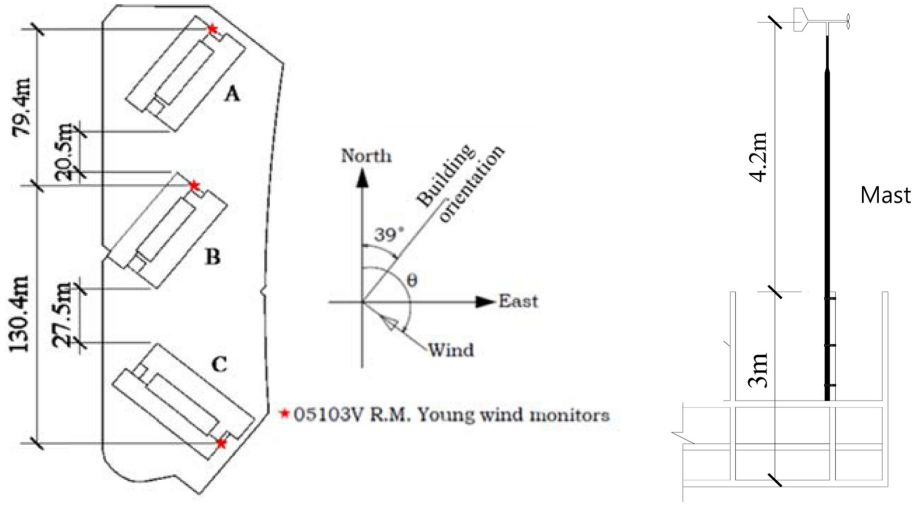


Figure 2. Arrangement of buildings and anemometers.

to gust wind for the propeller type and cup type anemometers (Brock and Richardson, 2001). The ratio R of the measured wind speed to the actual wind speed can be expressed as:

$$R_i = \frac{1}{\sqrt{1+(2\pi(\lambda/\lambda_i))^2}} \quad (1)$$

where R_i is the amplitude response ratio of the anemometer to the gust whose wavelength is λ_i. Eq.(1) indicates that short wavelength will lead to low R, which means the low accuracy of measurement. If the wavelength of a gust is 17m, then the recorded speed will be approximately 70.8% of the real speed. The response ratio is greater than 70.8%, when $\lambda_i > 17$ m. And the relation of wavelength and frequency is as follows:

$$\lambda_i = \frac{U}{f_i} \quad (2)$$

where U is the mean wind speed, and f_i is the frequency of the gust wave. According to Eqs. (1) and (2), the higher frequency means the shorter the wavelength, and lower amplitude response ratio of measurement. Therefore, although the sampling frequency was set to be 25.6 Hz during the measurement, the averaged data of every second is used for the analysis in this study.

The horizontal distance between measuring points on Buildings A and B is 80 m, and the line connecting these two points is about 6° shift to the west from the north direction. The distance between the measuring points on Buildings A and C is 210 m in plan. The wind direction is defined as 0° when the wind comes from the north, and the angle increases in the clockwise direction (Figure. 2).

3. Validation and selection of collected data

Based on the layout of anemometers, the wind speed at the measuring point may be affected by building or other attached components when wind approaches from certain directions. Thus, wind tunnel experiments were carried out in wind tunnel laboratory in Hunan University to check the effect of building on the wind speeds at the measuring point. The results of this experiment were used for validation and selection of the recorded data in full scale.

The arrangement of wind tunnel test is shown in Figure 3. Wind direction in the wind tunnel was defined the same as the full scale measurement (Figure. 2). The test target was Building-C in the test, as it is the highest one in the three buildings. If the wind speed above this building is not severely affected according to the experiment, then the wind speeds measured at the same position on the other two buildings will not be severely affected either. The geometrical scale was set to be 1:200 in this experiment. Wind speeds were measured by the cobra probe (Figure. 4) with sampling frequency 500 Hz. Wind speeds



Figure 3. Arrangement of wind tunnel simulation test.



Figure 4. The position of the cobra probe above building roof.

at various heights (5 cm, 7 cm, 10 cm, and 13 cm) above roof of Building-C were measured to compare with the wind speeds without buildings. These 4 heights correspond to 10 m (anemometer position), 14 m, 20 m, and 26 m above the roof in full scale. As the major object of this wind tunnel test was to investigate the effects of underneath building on the wind speed at the measuring point, only the open terrain was simulated in wind tunnel. Statistics of experiment results are shown in Table 1.

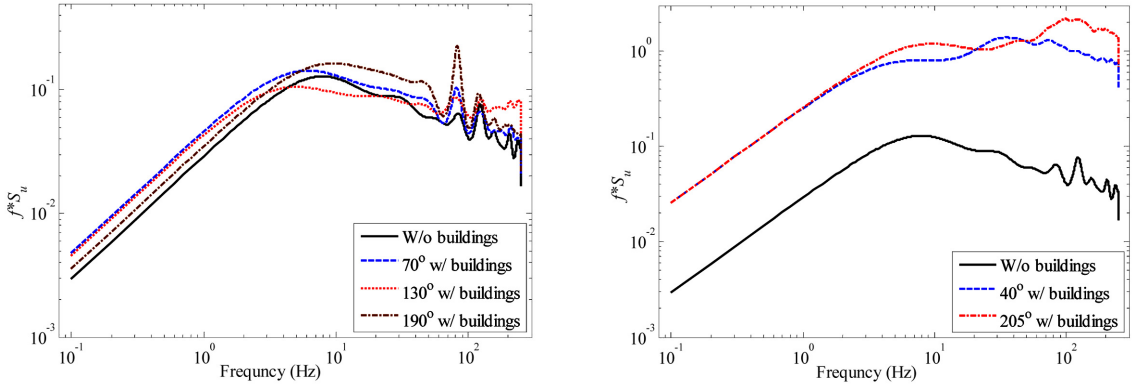
According to Table 1, the longitudinal mean wind speeds and turbulence intensities in the range [70°, 190°] could match the values of case without buildings well. The maximum difference of mean wind speed was (9.28-8.85)/ 8.85 × 100% = 4.9%. Although in case of 70° and 190°, the building had relatively strong effects on the lateral wind speeds, which led to about 7° difference in the wind direction, such deviation was basically tolerable. For the wind angles outside this range the turbulence increased very fast, which indicates that the measuring point is merged inside the high turbulent flow separated from the building roof.

The power spectra of longitudinal wind speeds under various wind directions were compared with the case without buildings as shown in Figure. 5. When wind direction

Table 1. Wind speed measured at 5cm above the building roof in wind tunnel test

Case	Wind direction	Mean wind speed (m/s)			Turbulence intensity (%)		
		U*	V*	W*	U*	V*	W*
W/o building	\	8.85	0.19	0.63	8.30	4.12	4.73
	40°	9.88	0.60	2.27	15.20	10.10	8.12
	55°	10.00	1.51	2.04	8.35	6.10	4.35
	70°	9.05	1.13	2.91	8.12	4.86	4.54
	85°	8.54	0.21	3.73	8.00	5.46	5.31
	100°	8.40	–0.38	4.52	7.59	5.32	5.91
	115°	8.29	–0.38	5.29	7.10	5.24	6.86
With buildings	130°	8.50	0.11	5.53	6.45	4.86	7.01
	145°	8.60	0.48	5.44	6.48	4.73	6.93
	160°	8.62	0.12	5.11	7.00	4.98	6.82
	175°	9.07	–0.30	4.22	7.16	4.88	5.56
	190°	9.28	–1.29	3.20	7.90	5.36	5.30
	205°	9.80	–2.51	1.36	17.30	9.89	7.55
	220°	6.50	–0.62	0.391	39.90	20.50	19.00

*U, V, W represents the longitudinal, lateral, and vertical wind direction respectively. Results of angle greater than 220° are not shown here, as the wind speeds at the measuring point are strongly affected by the building.



(a) 70°≤θ≤190° (b) θ<70° and θ>190°

Figure 5. The comparison of the power spectrum of longitudinal fluctuating wind of the case with buildings with the case without buildings.

was in the range of [70°, 190°], the power spectra agreed well with the case without buildings. Only when wind direction was around 130° (normal to the short side), the power spectrum showed more energy in the high frequency range than that without buildings. This may due to the interference from the strong vertical wind. When wind approached outside [70°, 190°], power spectrum deviated greatly from the without building case as shown in Figure. 5(b). This is because the wind speeds at the measuring points are affected by separated flow from underlying building.

Based on the results above, when wind approaches in the range of [70°, 190°], the longitudinal wind speeds recorded above Building-C are not severely affected by the underlying building, and can basically reflect the property of approaching flow, although the vertical wind speeds in the range [85°, 175°] are much higher than the case without buildings. Actually, according to the test results, even for the case wind speed was measured at 13 cm above the roof (26 m in full scale), more than 2 m/s upward mean wind speed could still be measured. That means the upward wind can hardly be avoided in this field measurement. However, the upward wind does not show strong interference effects on the longitudinal wind (Figure. 5(a)), which means the longitudinal wind speeds are still valid for analyzing the characteristics of incident wind in the range of [85°, 175°]. Wind speed data observed in field measurement will be selected based on this wind tunnel test to exclude the data that are severely affected by buildings.

The No. 19 tropical storm in 2013, the "Usagi", developed into a tropical storm at east of the Philippines on September 16th. "Usagi" intensified on September 19th and it ultimately became a violent and enormous typhoon. The system weakened slowly and it crossed the Bashi Channel on September 21st and landed in Guangdong

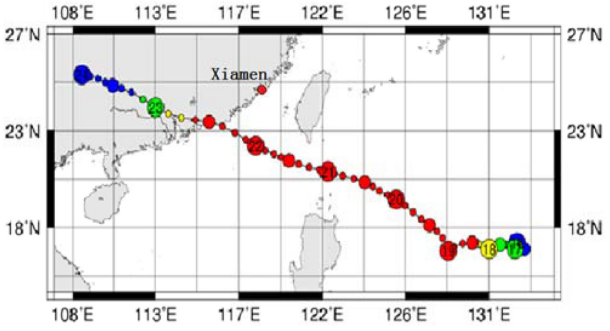


Figure 6. Track of Typhoon "Usagi", 16th-24th Sep., 2013.

Province, China on September 22nd. The closest distance from the typhoon center to the measurement site is about 270 km. Figure. 6 shows the track of the center of this typhoon published by National Institute of Informatics (2013). The wind data on top of the equipped buildings were collected from Beijing Time September 20th 7:55p.m. to September 23th 8:55a.m, with a total of 61 hours of data archiving the whole event of this typhoon. Figure. 7 shows the recorded wind speeds time series above the three buildings, while Figure. 8 shows the hourly mean wind directions which can be checked from about 30° to 140o. The time label "0" in the abscissa corresponds to 19:55 of Sep. 20th.

Figure. 7 shows that when wind approaches from particular ranges of direction, the turbulence of wind speed becomes very high, i.e. from 110° to 140° for Building-A, and from 30° to 70° for Building-C. This observation agrees well with the results of wind tunnel experiment. Based on both of the wind tunnel experiment and full scale measurement, the wind speed that are severely affected by the buildings are not used for the analysis. The unused wind speed data are shaded in Figure. 7. Comparing with the data collected on Building-A, strong turbulence can also be checked from the data recorded on Building-B, when wind direction was in the range of [30°, 50°]. According to Figures. 2 and 7(d), when wind comes from this direction range, Building-A is located at the upwind direction of Building-B. Under this condition, the measuring point on Building-B may be just inside the wake of Building-A, leading to the strong turbulence of wind speed.

4. Basic characteristics of wind speed

4.1 Turbulence intensity

In this section, the turbulence intensity is discussed in details. The data recorded on Building-A are adopted for checking the turbulence intensity. The turbulence intensity in this section is calculated based on every 10min long time interval data.

The relation of turbulence intensity and the mean wind

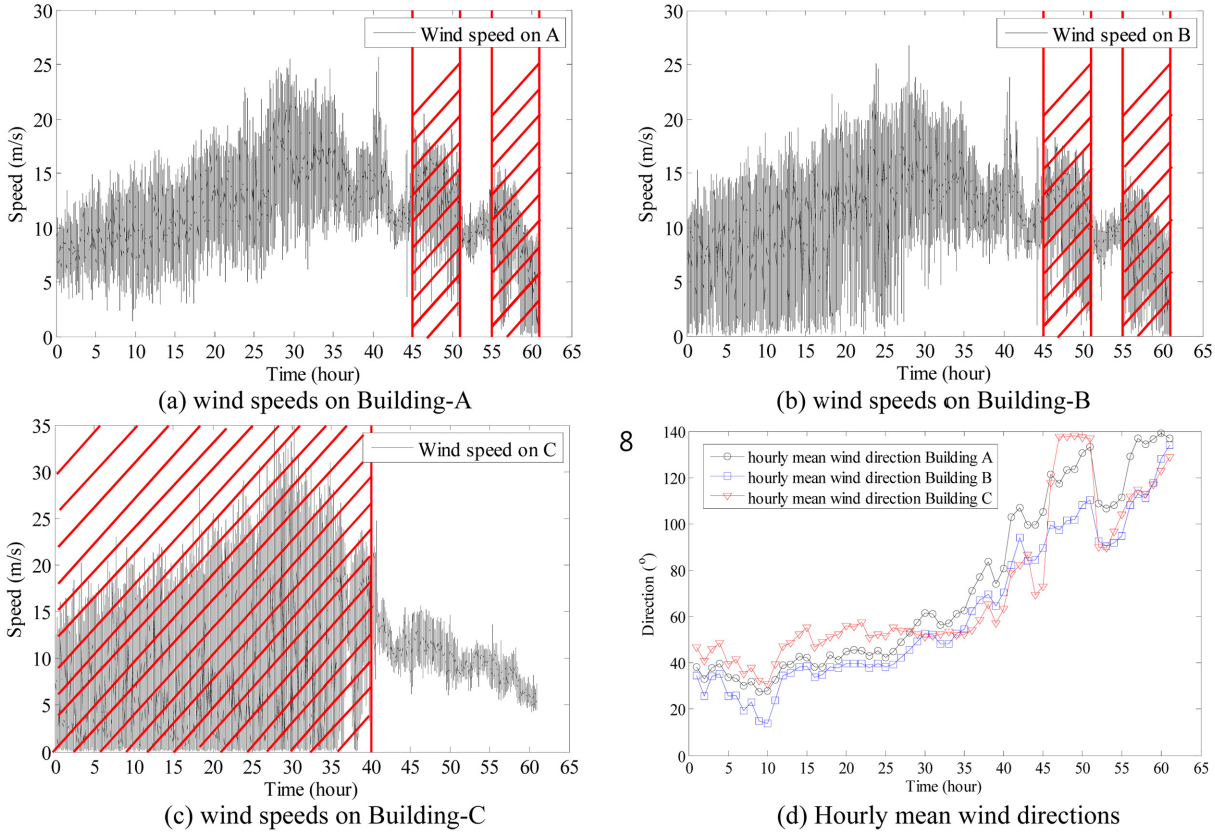
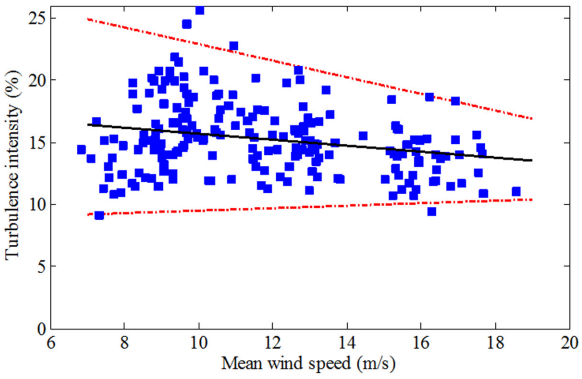
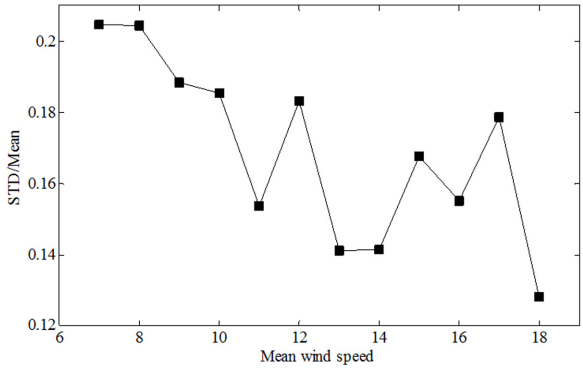


Figure 7. Recorded wind speeds on three buildings.



(a) Longitudinal turbulence intensity of 10min segments

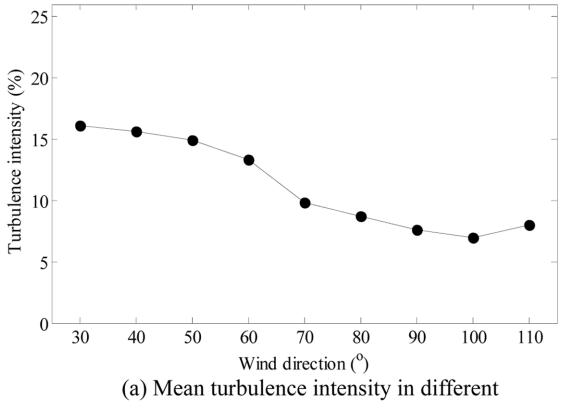


(b) Ratio of STD and mean turbulence intensity at each mean wind speed

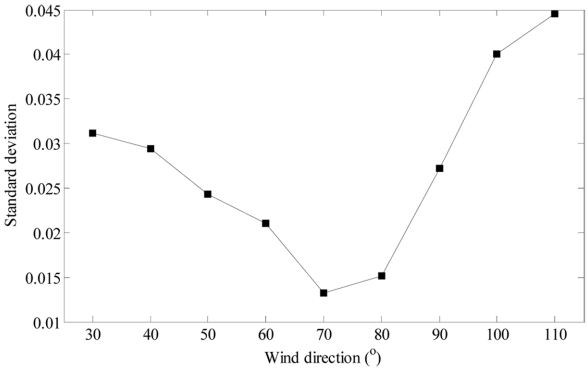
Figure 8. Longitudinal turbulence intensity versus mean wind speed.

speed is firstly examined. The terrain roughness in different directions of the monitored buildings is very different as described in Section 2. The first 35 hours of data from Building-A were selected, during which the wind directions were mainly located between 30° and 60°. The upwind terrain roughness does not change very much within this range. Thus, the terrain effects to the turbulence can be minimized. The longitudinal turbulence intensities are plotted against the corresponding 10min mean wind speeds in Figure. 8(a). The data were fitted by a linear function to describe the trend of mean values (black line), and the upper and lower linear boundaries indicate the trend of maximum and minimum values (dashed lines). Li, et al. (2014) discussed in more details about the estimation of turbulence intensity. The trend of mean turbulence intensity slightly decreases, in general, with an increase in the mean wind speeds. The upper boundary shows a larger reduction when the wind speeds increase, but the lower boundary maintains a zero slope. This result coincides with Cao et al. (2009), although the wind speeds are observed at different heights in the two studies. Based on the measured wind speed data above Central Plaza Tower (374 m) in Hong Kong and Di Wang Tower (384 m) in Shenzhen, Li et al. (2005) also pointed out that with the increase of mean wind speed, the turbulence intensity decreases. This tendency can also be observed in this study. The ratios between standard deviation (STD) and mean of turbulence intensity for different wind speeds are shown in Figure. 8(b). This ratio gradually decreased with the mean wind speed from more than 0.2 to less than 0.13. The results show that turbulence intensities exhibit a very scattered distribution in the real situation, even though the scatter weakens with the increase of mean wind speed. This large scatter may result occasionally in more severe wind loads and pressures on structures than those estimated by using the turbulence intensity in codes or in wind tunnel experiments. It is therefore necessary to consider such strong non-stationary phenomenon in the analysis of wind induced vibration and extreme wind pressures on claddings.

The mean turbulence intensity changes with the incident wind direction as shown in Figure. 9(a). The mean turbulence decreases slightly when θ changed from 30° to 50°. Then there is a sharp decrease from the 15% to 9% when θ changed from 50° to 80°. When θ was in the division 80°



(a) Mean turbulence intensity in different wind directions



(b) Standard deviations of turbulence intensity in different wind directions

Figure 9. Change of turbulence intensity with wind direction.

to 110° the mean turbulence intensity stayed below 9%. This diagram clearly depicts the effects of upwind terrain roughness to the turbulence intensity.

The standard deviation of the scattered turbulence intensities within each 10° division of wind direction was also checked as shown in Figure. 9(b). When typhoon center was moving away, the variation of turbulence intensity was higher than the case when it was approaching, which may imply stronger non-stationarity of wind speed.

Turbulence intensity of wind is a critical parameter for estimating wind load on structures. From the analysis in this section, it is found that many factors can affect the turbulence intensity, i.e. wind speed, upwind terrain and also the relative location to the Typhoon center. Thus, more attentions are needed for it while wind load are considered for structure design.

4.2 Turbulence integral scale

Turbulence integral scale is also one of the basic parameter used in structure engineering, as the longitudinal integral scale represents the average along-wind dimension of the wind gusts in a given data segment. The gust size increases, means its influence on a structure increases.

The equation of calculating integral scale is as follows:

$$L = \frac{\overline{U}}{\sigma^2}\int_0^T R(t)dt \tag{3}$$

where σ^2 is the variance of fluctuating wind speed; T is the duration of the data series; $\overline{U}$ is the corresponding longitudinal mean wind speed; $R(t)$ is the auto-covariance function of the fluctuating longitudinal wind speed. Figure. 10 shows the estimated turbulence scale based on the 10min and 1hour duration from the 21st to 45th hour on Building-A. One of the problem for evaluating the turbulence scale of field measured wind speed is that 10min long records may not be long enough to get stable results, because the results of 10min duration fluctuate strongly as shown. However, if it is estimated based on every 1hour long records, the low frequency trend component may severely distort the calculated results from the credible range. Results show that the turbulence scales from 35th to 45th hour became quite large which can even exceed 2000 m. Such results are clearly abnormal for the turbulence scale at about 100m high.

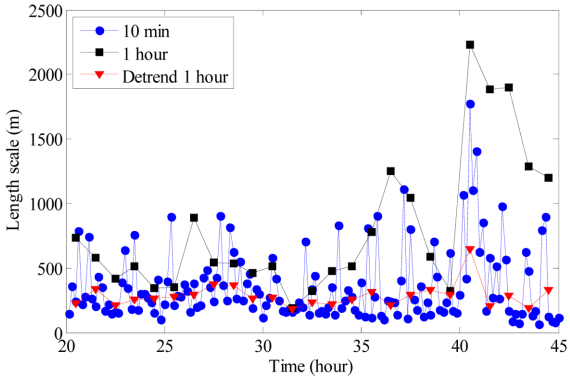


Figure 10. Turbulence length scale from different methods.

The study made by Xu and Chen (2004) found that the non-stationary time varying mean wind speed may affect the characteristics of wind speed severely. Thus, in order to remove the effect from low frequency trend component, the Discrete Wavelet Transform (DWT) technique was adopted to decompose the wind speed data and extract the low frequency component (Hui, et al., 2017). DWT uses a couple of filters —high pass ($h[k]$) and low pass ($g[k]$) filters—to decom-pose the signal $x[n]$ into two frequency sub-bands, each of them occupies half band of the original frequency range. The algorithm of the first stage decomposition can be expressed as:

$$x_{1,L}[n] = \sum_{k=0}^{K-1} x[2m-k]g[k] \tag{4}$$

$$x_{1,H}[n] = \sum_{k=0}^{K-1} x[2m-k]h[k] \tag{5}$$

where K is the length of digital filters $g[k]$ and $h[k]$, $x_{1,L}[n]$ is named as the approximate coefficients, and occupies the lower half frequency range, and $x_{1,H}[n]$ is named as the detailed coefficients, and occupies the higher half frequency range. Further decomposition (from the $(a-1)$th level to the ath level) is:

$$x_{a,L}[n] = \sum_{k=0}^{K-1} x_{a-1,L}[2n-k]g[k] \tag{6}$$

$$x_{a,H}[n] = \sum_{k=0}^{K-1} x_{a-1,L}[2n-k]h[k] \tag{7}$$

A 9-level wavelet decomposition was applied to the whole 61 hours wind speed time series. "Daubechies wavelet" (Daubechies, 1992) was adopted to decompose the data. The approximate coefficients of the 9th level DWT were extracted from the time series. This means the low frequency information within $(0, 2^{-10})$ Hz, which can be considered as the trend component, was filtered out from the data. Figure. 11 shows the trend component of record from Building-A. From 35th to 45th hour, the strong fluctuations of the low frequency component can be clearly checked. Therefore, as shown in Fig.10 the turbulence scales during this period without detrending process become quite large, no matter based on 10min or 1 hour time interval.

By removing the trend from the original data, the turbulence length scale is re-estimated according the

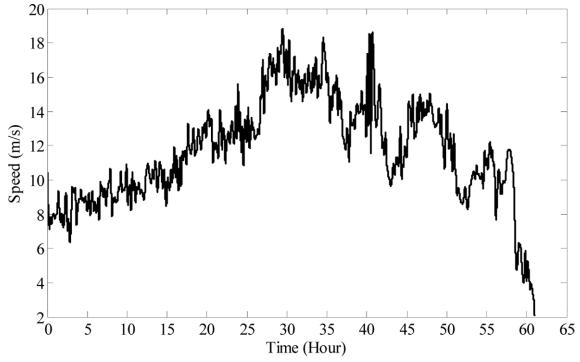


Figure 11. Trend of wind speed records on Building-A.

following equation:

$$L = L = \frac{\overline{U}}{\sigma^2}\int_0^T R_{dt}(t)dt \tag{8}$$

where σ_{dt}^2 is the variance of detrended wind speed, $R_{dt}(t)$ is the auto-covariance function of detrended wind speed. The re-estimated results by adopting Eq. (8) are also shown in Figure. 10, based on every 1 hour duration's data. After this detrending process, the estimated scales are about 200 m to 250 m at 100 m high for this typhoon, these results are much more stable and reliable than the results estimated without detrending process.

4.3 Power spectrum

The power spectrum was calculated based on every one hour wind speed data, and the longitudinal wind power spectra of different mean incident wind directions were checked. The power spectra of wind speeds within every 10° division of mean wind direction were averaged and compared with Von Karman spectrum in this Section. Taking the division [55°, 65°] as an example, totally 7 samples were selected for calculating the spectrum. The wind speed information of the 7 samples are shown in Table 2.

The power spectra in each division are shown in Figure. 12. The power spectrum of the observed data and the Von Karman model matched well when wind came in the direction 35° to 45°. The difference tended to be larger with an increase in the angle. According to the comparison with Karman spectrum, it can be checked that the major differences concentrate at the low frequency range. Such results clearly indicate that when the typhoon center was approaching (incident wind angel smaller than 50°), wind speed can match with Karman spectrum well. However, after typhoon made landfall, and moved forward into inland, the low frequency fluctuation of wind speed gradually increased making the power spectrum deviate from Karman spectrum. The low frequency fluctuation can also be seen in Figure. 11. After the 35th hour, the fluctuation of trend became much stronger than the first 35 hours'.

5. Cross correlation of wind speeds

Since the three anemometers recorded the data simultaneously, the data collected from Buildings A and B are applied to study the cross correlation in details. As the wind speeds measured above Building C were severely contaminated for a very long period, the cross correlation between the data measured on Buildings A and C, and on Buildings B and C are not checked herein.

The cross-correlation coefficients of the wind speeds measured on Buildings A and B for each 10min were calculated base on the following equation

$$R_{xy}(\Delta t) = \frac{C_{xy}(\Delta t)}{\sqrt{C_{xx} \cdot C_{yy}}} \tag{9}$$

where C_{xx} and C_{yy} are the variance of $x(t)$ and $x(t)$ respectively. $C_{xy}(\Delta t)$ is the cross-covariance of $x(t)$ and $y(t)$ which is calculated as follow:

$$C_{xy}(\Delta t) = E[(x(t)-\bar{x})(y(t+\Delta t)-\bar{y})] \tag{10}$$

According to Eq. (9), $R_{xy}(\Delta t)$ is a function of Δt, which is also known as time lag. Figure. 13(a) shows the maximum $R_{xy}(\Delta t)$ of each 10min long segment data in the along-wind direction (with respect to the 10min mean wind direction). For the first 35 hours when typhoon center was approaching, and the incident wind directions were mainly smaller than 60°, the maximum $R_{xy}(\Delta t)$ in the along-wind direction tended to increase with wind speeds from around 0.4 to 0.7. When the wind speeds started to decrease, the coefficients decreased accordingly to around 0.2. Figure. 13(b) shows that the maximum coefficients of the across wind. Different from the along-wind direction, the cross correlation did not show clear dependence on

Table 2. Data information for calculating power spectrum in direction interval [55°, 65°]

Time	Data source	Mean direction (°)	Mean speed (m/s)	Turbulence intensity
29th Hour	Building-A	58	16.6	15.4%
30th Hour	Building-A	62	17.5	14.3%
31st Hour	Building-A	61	16.2	14.4%
32nd Hour	Building-A	56	15.6	13.2%
33rd Hour	Building-A	57	15.7	12.9%
34th Hour	Building-A	61	15.9	11.9%
35th Hour	Building-A	63	16.6	13%

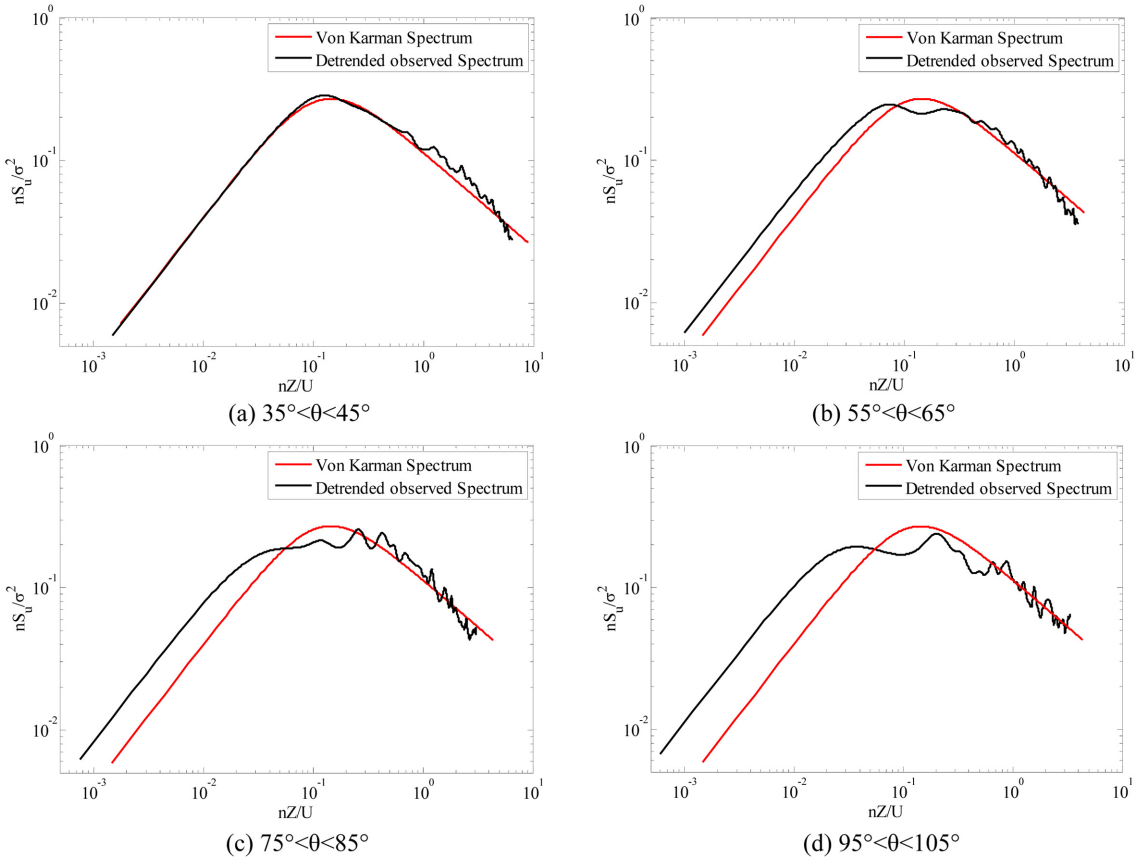


Figure 12. Power spectrum of detrended wind speed in different directions.

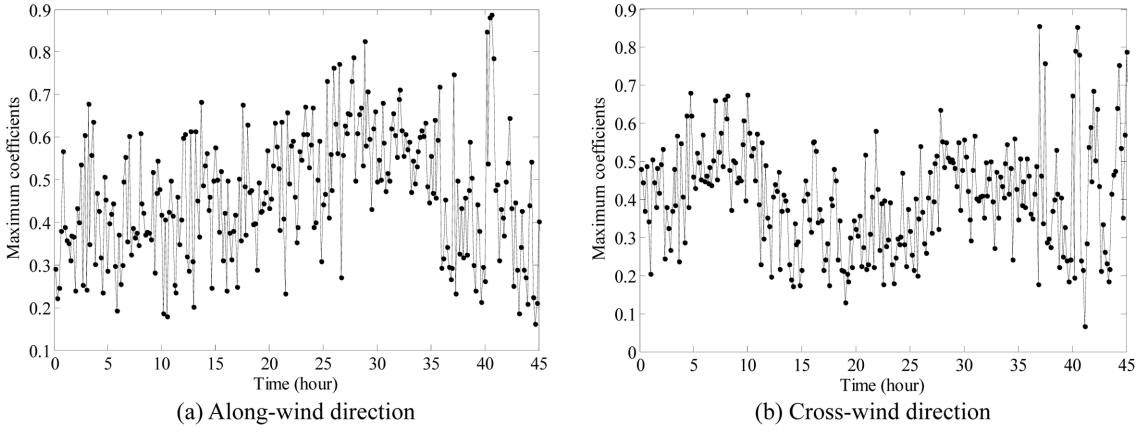
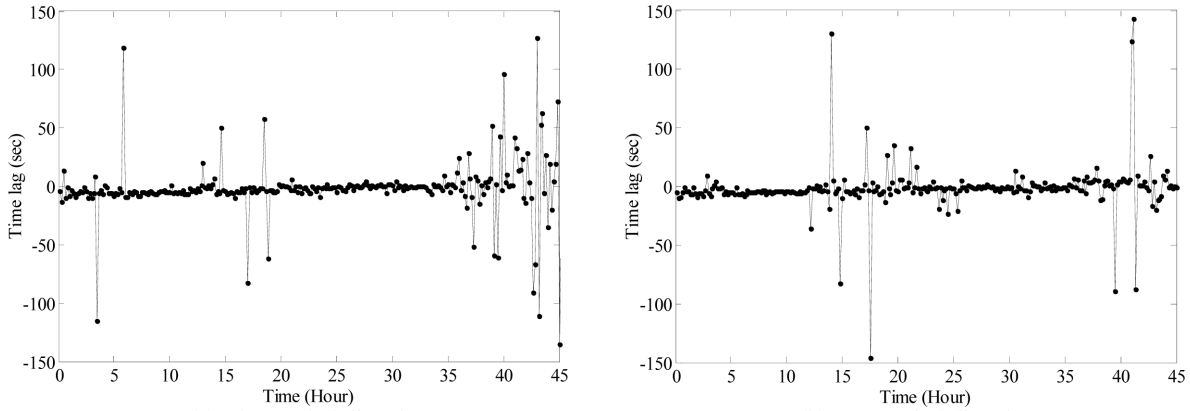


Figure 13. Maximum cross-correlation coefficients

wind speed.

It may be concluded from the above analysis that when the wind comes from the city terrain (northeast side), the cross correlations of the wind speeds at the two points are generally high in the along-wind direction, and the correlations tend to increase with the increase of wind speed. When wind comes directly from the open terrain (east side), the longitudinal cross correlation between the two points become weak, but the cross-wind cross correlation becomes strong.

Figure. 14 shows the time lags Δt corresponding to the maximum $R_{xy}(\Delta t)$ for each 10min interval varies with time. Δt can basically be interpreted as the time of a gust moving from measuring point above Building-A to Building-B. For the first 35 hours, the time lags were very stable no matter in the along-wind direction or in the cross-wind direction, with its value gradually shifting from around 10sec to 0sec. Such changes indicate that at

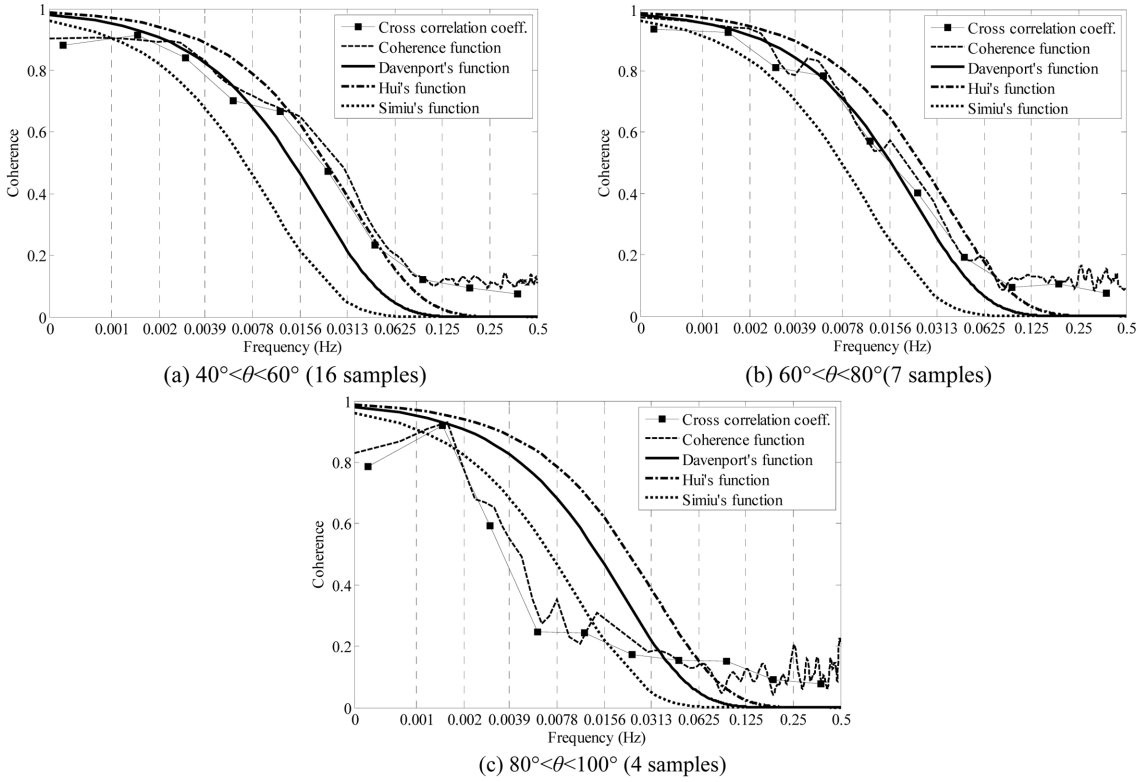


(a) Along-wind direction (b) Cross-wind direction

Figure 14. Time lag of the maximum cross-correlation coefficients.

the beginning of the storm the incident gust attacked Building-A before Building-B, with the moving of typhoon center and the change of wind direction the gust wind attacked the two buildings almost at the same time. For the along-wind direction, when wind speeds started to decrease and the wind direction was greater than 60°, the time lags of the maximum coefficients became very unstable and varied in a wide range. These results may due to the fact that the spatial correlation of wind speeds at the two positions was very weak during this period, so that time lag could not be well evaluated. For the cross-wind direction, the time lag after the 35th hour were still kept around 0.0sec which was more stable than the along-wind direction. That means the cross correlation in cross-wind direction do depend strongly on the wind speed and wind direction.

The cross-correlation between measured longitudinal wind speeds were also checked in different frequency bands by adopting DWT. The 9-level DWT was applied to the whole 61 hours of wind speeds data measured above Buildings A and B by using "Daubechies wavelet". Each sample was decomposed into 10 components, with one approximation component of the 9th level that occupies [0, 2^{-10}]Hz, and 9 levels' detail components with the i^{th}



(a) 40°<θ<60° (16 samples) (b) 60°<θ<80°(7 samples)

(c) 80°<θ<100° (4 samples)

Figure 15. Cross correlation in frequency domain and coherence function.

level occupies [$2^{-(i+1)}$, 2^{-i}]Hz. For each frequency sub-band component, the cross correlation coefficients were calculated hour by hour. $R_{xy}(0)$ for each frequency sub-band were retained and averaged for samples whose mean incident wind directions are within a 20° range. Results are plotted in frequency domain as shown Figure. 15. Each data point shown in the diagram indicates a mean cross correlation coefficients in the frequency band marked by the nearby bounding vertical gridlines. When the frequency was low, the cross correlation was strong and the coefficients were close to unity. And the coefficients decreased with the increase of frequency for all cases. When θ was smaller than 80° the cross correlation decayed slowly with frequency. And while θ was greater than 80°, the decaying speed became faster comparing to other cases.

The coherence functions were also calculated according to Eq. (11) for comparison,

$$Coh(n)=\frac{\left|S_{u_iu_j}(n)\right|}{\sqrt{S_{u_i}(n)S_{u_j}(n)}} \tag{11}$$

where $S_{u_iu_j}(n)$ is cross power spectrum, $S_{u_i}(n)$ and $S_{u_j}(n)$ are the auto power spectrum of wind speeds at point i and j.

The averaged coherence functions of different wind directions are also shown in Figure. 15, which show good agreement with the results obtained by calculating cross correlation coefficient in different frequency bands. It is known that

$$C_{xx}=\int S_x(n)dn \tag{12}$$

Comparing Eqs. (9) and (11), according to Eq. (12) the cross correlation coefficients $R_{xy}(0)$ in each frequency sub-band is equivalent to the coherence function

Because the conventional Fourier Transform (FT) method cannot change frequency resolution, the calculated coherence function can hardly be well evaluated simultaneously in the whole frequency ranges. One advantage of this newly proposed method for evaluating coherence function is that it can evaluate coherence function with flexible frequency resolutions. The frequency resolution can be set to gradually become finer while the frequency approaches 0.0 Hz.

The coherence experience function was originally proposed by Davenport (1961). The expression of the Davenport model is

$$Coh(r,n)=\exp\left(-\frac{n}{v_z}\sqrt{c_x^2(x_i-x_j)^2+c_z^2(z_i-z_j)^2}\right) \tag{13}$$

where r is the distance between two points, x_i, x_j, z_i, z_j are the horizontal and vertical coordinates of the two points. c_x and c_z are two parameters which are 8.0 and 7.0 recommended by Davenport. After that, many studies have tried to give a better function to represent the spatial coherence. Simiu and Scanlan (1996) adopted Eq. (13), but c_x and c_z are 16.0 and 10.0 instead based on their study. Hui et al (2009b) also gave spatial coherence function of longitudinal wind speed based on their long term observation shown as follows:

$$Coh(r,n)=\exp\left(-\frac{n}{v_z}\sqrt{c_x^2(x_i-x_j)^2+c_y^2(y_i-y_j)^2+c_z^2(z_i-z_j)^2}\right) \tag{14}$$

where c_x, c_y and c_z are 5.19, 4.49 and 7.28. x, y, z represent the lateral, longitudinal wind direction and vertical direction respectively. Based on the introduction above, the coherence experience function cannot be easily concluded, though the basic form has been widely used. All the three models are also shown in Figure.15 to compare with the results of this study.

When the wind direction θ<80°, the observed results could mainly located in the range of three models covering, and matched the experience function relatively well. However, when θ>80°, the observed results showed great difference with all the models. These results indicate that besides the spatial distance, wind speeds and wind direction, some other factors such as the upwind terrain roughness and non-stationary wind might also affect the decaying speed of the coherence of data from two positions. More wind speeds records and studies are still needed, before an appropriate model to describe the coherence of wind speeds in typhoon can be set.

6. Conclusions

Wind speeds above three high-rise buildings in Xiamen city, China were measured during the Typhoon "Usagi". Some characteristics of the wind speeds were examined based on the recorded wind speeds data in this study. The field measurement results were also validated by wind tunnel experiment. Conclusions are summarized below:

(1) Turbulence intensity at the height of 108 m was studied. Results show that with a change of incident wind direction, the turbulence intensities vary in a very wide range from 16% to 7% because of the change of upwind terrain. Such results reflect the big changes of the terrain roughness surrounding the building. Both mean and variance of turbulence intensity decreased with the increase of mean wind speed.

(2) Non-stationary property of typhoon in the very low frequency component [0, 2^{-10}]Hz (the trend information) was studied by adopting DWT. When the typhoon approached from the sea, wind speed increased in a smooth way; after landing and moving into land, wind speed decreased with strong fluctuations in low frequencies. By removing the low frequency component, the turbulence integral scale became much more stable and reasonable than the original data. And the Low frequency component was found to constitute the major difference of typhoon spectrum from the Karman spectrum.

(3) The cross correlation between the measured data above Buildings A and B was also checked. For the longitudinal component, it was found that the cross correlation became stronger when the wind speeds increased. When typhoon center moved away the spatial correlation of two point became very weak. For the lateral component, the wind speed did not show strong effects on the cross correlations. A method of evaluating coherence function was developed. And coherences of the wind speeds under different incident wind directions were also examined. Results were compared with some experience coherence functions also, which showed that many factors also affect the decaying speed of the coherence besides the distance and wind speeds of the two positions, and further studies on this topic may still be needed.

7. Acknowledgement

This study is supported by 111 project (B18062) and Chongqing Postdoctoral Science Foundation (XmT2018039). The authors give special thanks to Prof. Q.S. Yang and Prof. S.S. Law for their great help.

References

Brock, F. V., Richardson, S. J. (2001). *Meteorological measurement systems*, Oxford University Press, New York, USA.

Cao, S., Tamura, Y., Kikuchi, N., Saito, M., Nakayama, I., Matsuzaki, Y. (2009). Wind characteristics of a strong typhoon, *J. Wind Eng. Ind. Aerodyn*, 97(1), 11-21.

Davenport, A. G. (1961). The Spectrum of Horizontal Gustiness near the Ground in High Winds, *Q. J. R. Meteorol. Soc*, 87, 194-211.

Daubechies, I. (1992). *Ten lectures on wavelets*, SIAM, Philadelphia, PA.

Fu, J. Y., Li, Q. S., Wu, J. R., Xiao, Y. Q., Song, L. L. (2008). Field measurements of boundary layer wind characteristics and wind-induced responses of super-tall buildings, *J. Wind Eng. Ind. Aerodyn*, 96(8-9), 1332-1358.

Hui, M. C. H., Larsen, A., Xiang, H. F. (2009a). Wind turbulence characteristics study at the Stonecutters Bridge site: Part I-Mean wind and turbulence intensities. *J. Wind Eng. Ind. Aerodyn*, 97(1), 22-36.

Hui, M. C. H., Larsen, A., Xiang, H. F. (2009b). Wind turbulence characteristics study at the Stonecutters Bridge site: Part II: Wind power spectra, integral length scales and coherences, *J. Wind Eng. Ind. Aerody.*, 97(1), 48-59.

Kijewski-Correa, T., Kareem, A., Guo, Y. L., Bashor, R., Weigand, T. (2013). Performance of tall buildings in urban zones: lessons learned from a decade of full-scale monitoring, *Int. J. High-rise Build*, 2(3), 179-192.

Kim, W., Tamura, Y., Yoshida, A. (2011). Interference effects on local peak pressures between two buildings, *J. Wind Eng. Ind. Aerodyn*, 99, 584-600.

Li, Q. S., Li, X., and He, Y. C. (2016). Monitoring wind characteristics and structural performance of a super-tall building during a landfall typhoon. *J. Struct. Eng.*, 142(11), 04016097.

Li, Q. S. Xiao, Y. Q., Wong, C. K. (2005). Full-scale monitoring of typhoon effects on super tall buildings, 20, 697-717.

Li, Q. S., Xiao, Y. Q., Wu, J. R., Fu, J. Y., Li, Z. N. (2008). Typhoon effects on super-tall buildings, *J. Sound Vib*, 313, 581-602.

Li, S. W., Tse, K. T., Weerasuriya, A. U., Chan, P. W. (2014). Estimation of turbulence intensities under strong wind conditions via turbulent kinetic energy dissipation rates, *J. Wind Eng. Ind. Aerodyn*, 131, 1-11.

Li, X., & Li, Q. S. (2019). Observations of typhoon effects on a high-rise building and verification of wind tunnel predictions, *J. Wind Eng. Ind. Aerodyn*, 184, 174-184.

Masters, F. J., Tieleman, H. W., Balderrama, J. A. (2010). Surface wind measurements in three Gulf Coast hurricanes of 2005, *J. Wind Eng. Ind. Aerodyn*, 98 (10-11), 533-547.

National Institute of Informatics, Typhoon 201319 (USAGI). http://agora.ex.nii.ac.jp/digital-typhoon/summary/wnp/s/201319.html.en.

Schroeder, J., Smith, D. (2003). Hurricane Bonnie wind flow characteristics as determined from WEMITE, *J. Wind Eng. Ind. Aerodyn*, 91, 767-789.

Schroeder, J., Edwards, B., Giammanco, I. (2009). Observed tropical cyclone wind flow characteristics, *Wind Struct*, 12(4), 347-379.

Simiu, E., and Scanlan, R. (1996). Wind effects on structures: fundamentals and application to design (Third Edition), John Wiley and Sons, New York, USA.

Tamura, Y., Shimada, K., Hibi, K. (1993). Wind response of a tower (Typhoon observation at the Nagasaki Huis Ten Bosch Domtoren). *J. Wind Eng. Ind. Aerodyn*, 50, 309-318.

Tse, K. T., Li, S. W., Chan, P. W., Mok, H. Y., Weerasuriya, A. U. (2013). Wind profile observations in tropical cyclone events using boundary layer wind-profilers and doppler SODARs, *J. Wind Eng. Ind. Aerod*, 115, 93-103.

Tse, K. T., Li, S. W., Qin, C. Q., Chan, P. W. (2014). Wind characteristics observed in the vicinity of tropical cyclones: An investigation of the gradient balance and super-gradient flow, *Wind Struct*, 19(3), 249-270.

Vickery, P., Skerlj, P. (2005). Hurricane gust factors revisited, *J. Struct. Eng*, 131(5), 825-832.

Wang, B., Hu, F., Cheng, X. (2011). Wind gust and turbulence statistics of typhoons in South China, Acta Meteorol. Sin, 25(1), 113-127.

Wang, H., Li, A., Niu, J., Zong, Z., Li J. (2013). Long-term monitoring of wind characteristics at Sutong Bridge site, *J. Wind Eng. Ind. Aerodyn*, 115, 39-47.

Xu, Y. L., and Chen, J. (2004). Characterizing nonstationary wind speed using empirical mode decomposition. *J. Struct. Eng*., 130, 921-920.

Xu, Y. L., Zhan, S. (2001). Field measurements of Di Wang tower during typhoon York, *J. Wind Eng. Ind. Aerodyn*, 89(1), 73-93.

Yoshida, A., & Tamura, Y. (2015). Field measurement and modal identification of various structures for structural health monitoring. Int. *J. High-rise Build*, 4(1), 9-25.